

Coupling the advection-dispersion equation with fully kinetic reversible/irreversible sorption terms to model radiocesium soil profiles in Fukushima Prefecture

Hiroshi Kurikami^{1*}, Alex Malins², Minoru Takeishi³, Kimiaki Saito⁴, Kazuki Iijima⁵

¹Japan Atomic Energy Agency (JAEA), Sector of Fukushima Research and Development, 10-2 Fukasaku, Miharu-machi, Tamura-gun, Fukushima 963-7700, Japan, kurikami.hiroshi@jaea.go.jp, Tel: +81-247-61-2910

²Japan Atomic Energy Agency (JAEA), Center for Computational Science & e-Systems, University of Tokyo Kashiwanoha Campus Satellite, 178-4-4 Wakashiba, Kashiwa, Chiba 277-0871, Japan, malins.alex@jaea.go.jp

³Japan Atomic Energy Agency (JAEA), Sector of Fukushima Research and Development, 10-2 Fukasaku, Miharu-machi, Tamura-gun, Fukushima 963-7700, Japan, takeishi.minoru@jaea.go.jp

⁴Japan Atomic Energy Agency (JAEA), Sector of Fukushima Research and Development, 2-2-2 Uchisaiwai-cho, Chiyoda, Tokyo 100-8577, Japan, saito.kimiaki@jaea.go.jp

⁵Japan Atomic Energy Agency (JAEA), Sector of Fukushima Research and Development, 10-2 Fukasaku, Miharu-machi, Tamura-gun, Fukushima 963-7700, Japan, iijima.kazuki@jaea.go.jp

*Corresponding author

- A Diffusion-Sorption-Fixation model with kinetics for reversible sites is proposed.
- Model reproduces initial exponential depth distribution of radiocesium in soil.
- Initial relaxation mass depends on K_d , kinetic rate and dispersion coefficient.
- Differing sorption and desorption rates cause long tails in distribution at large depths.
- High organic matter content near surface can explain activity peaks below ground.

Abstract

Radiocesium is an important environmental contaminant in fallout from nuclear reactor accidents and atomic weapons testing. A modified Diffusion-Sorption-Fixation (mDSF) model, based on the advection-dispersion equation, is proposed to describe the vertical migration of radiocesium in soils following fallout. The model introduces kinetics for the reversible binding of radiocesium. We test the model by comparing its results to depth profiles measured in Fukushima Prefecture, Japan, since 2011. The results from the mDSF model are a better fit to the measurement data (as quantified by R^2) than results from a simple diffusion model and the original DSF model. The introduction of reversible sorption kinetics means that the exponential-shape depth distribution can be reproduced immediately following fallout. The initial relaxation mass depth of the distribution is determined by the diffusion length, which depends on the distribution coefficient, sorption rate and dispersion coefficient. The mDSF model captures the long tails of the radiocesium distribution at large depths, which are caused by different rates for kinetic sorption and desorption. The mDSF model indicates that depth distributions displaying a peak in activity below the surface are possible for soils with high organic matter content at the surface. The mDSF equations thus offers a physical basis for various types of radiocesium depth profiles observed in contaminated environments.

Key words

Fukushima NPP accident, radiocesium vertical distribution, modified Diffusion-Sorption-Fixation model, exponential distribution, sorption kinetics

1. Introduction

The accident at the Fukushima Dai-ichi Nuclear Power Plant contaminated land across Fukushima Prefecture (Evrard et al., 2015). The main nuclide of concern over the long-term from the perspectives of radiation protection and radioecology is the radiocesium isotope ^{137}Cs , which is a characteristic component of nuclear weapons-testing and reactor accident fallout. Soil consists of organic and inorganic matter that have various microscopic binding sites for radiocesium. It is well known that frayed edge sites of micaceous minerals strongly bind radiocesium (e.g., Okumura et al., 2013; Fuller et al., 2015). On the other hand, Mukai et al. (2014) reported that radiocesium sorption was not limited to frayed edge sites but occurs uniformly on weathered biotite. Murota et al. (2016) reported evidence for several radiocesium binding sites on Fukushima soil particles.

Despite its affinity for binding to soil, radiocesium gradually migrates deeper into the ground over time (Gale et al., 1964). This results in a faster rate of reduction of air dose rates (groundshine) than would otherwise be expected by radioactive decay (International Commission on Radiation Units and Measurements (ICRU), 1994; Saito and Onda, 2015; Mikami et al., 2015; Malins et al., 2016). The depth profile and fixation of radiocesium in soil affects its uptake by vegetation (Beresford et al., 1992; Krouglov et al., 1996) and its redistribution by soil erosion and sediment transport (He and Walling, 1997). It is important therefore to understand the physiochemical processes altering radiocesium depth distributions in soil to predict how they will evolve over time and to evaluate countermeasures against the contamination.

Measured profiles of the radiocesium activity with depth in soil are often fitted with empirical functions such as the exponential for the years following fallout (Beck, 1966; ICRU, 1994). This facilitates the extraction of parameters characterizing the penetration of the

contamination into the soil, such as relaxation masses per unit area. Yesin and Cakir (1989), Clouvas et al. (2013), Matsuda et al. (2015), Takahashi et al. (2015) and Malins et al. (2016) are examples of such studies after the Chernobyl and Fukushima nuclear accidents.

Compared to the single exponential, Antonopoulos-Domis et al. (1995) showed that depth profiles of Chernobyl radiocesium in Northern Greece were better fitted as the sum of two exponentials, corroborating experiments by Ohnuki and Tanaka (1989). Some radiocesium depth profiles from Fukushima Prefecture also display this two exponential characteristic, where there is a steep decrease in the radiocesium activity below the surface of the ground, followed by a long tail in the distribution deeper in the soil (e.g., Matsuda et al., 2015; Takahashi et al., 2015). A third class of empirical functions, such as the Lorentz (Hillmann et al., 1996) and the hyperbolic secant (Matsuda et al., 2015), are fitted to depth profiles displaying a peak in radiocesium activity below the surface. The drawback of empirical models for the depth distribution is that they do not offer a physical basis for the formulae they employ. A similar criticism has been noted against compartment models for the radiocesium depth profile (Kirchner, 1998).

Various physiochemical models have been proposed for the evolution of radiocesium distributions within soil. Typically the models describe how the distribution along one direction (the depth direction) changes over time. The radiocesium inventory reduces by radioactive decay. Bossew and Kirchner (2004) summarized the various assumptions and limitations inherent in these models, such as the assumption of constant physical (e.g. soil density) and chemical (e.g. distribution coefficients) parameters over both soil depth and time. The main differences between the models lie in the number and types of sorption sites for radiocesium, the use of explicit kinetic terms to model sorption processes, and the inclusion of advective transport. Table 1 summarizes the key physiochemical models from the literature and the differences between them.

In the simplest case, the radiocesium migration is modelled as a diffusion process of the fraction dissolved within soil pore water (simple diffusion model, Table 1). A reversibly-sorbed fraction is in instantaneous equilibrium with the dissolved fraction, at a ratio set by a chemical distribution coefficient. The solution of this model for a pulse-like initial input of fallout is a Gaussian distribution. However, this function is not ideal for modeling the exponential-shape profiles frequently observed in the field (Bossew and Kirchner, 2004).

Antonopoulos-Domis et al. (1995) succeeded in reproducing the long tail deep in the soil profile seen in radiocesium distributions in the field with a Diffusion-Fixation (DF) model. The model introduced an advection term for the migration of radiocesium in pore water, and a kinetic model for radiocesium binding irreversibly to a single soil binding site (Table 1). The main drawback of the model is that it does not adequately capture the gradual migration of radiocesium deeper into the ground over time.

Toso and Velasco (2001) proposed a Diffusion-Sorption-Fixation (DSF) model, which increased the number of possible sorption sites to two. It considered a reversible sorption site, with instantaneous equilibration between the dissolved and reversibly sorbed fraction, as per the simple diffusion model (Table 1). The model then introduced a second sorption site for irreversible binding of radiocesium. The kinetics of fixation were modelled explicitly using a pseudo-first order chemical reaction term. Although advective transport was neglected, the DSF model captured the exponential distribution at the terminal state. However, it could not describe the exponential distribution seen in the early stages following fallout as well as the DF model. The DSF model is similar to the two-site model proposed by van Genuchten and Wagenet (1989) for pesticide transport and degradation in farmland soils.

The assumption of instantaneous equilibration between dissolved and reversibly sorbed radiocesium (simple diffusion and DSF models, Table 1) is limiting when trying to understand

short term, dynamic, phenomena such as the depth profile immediately following fallout deposition (Bossey and Kirchner, 2004; International Atomic Energy Agency (IAEA), 2009). Recently long term laboratory desorption tests of radiocesium from Fukushima soils have provided evidence of sorption sites with different kinetic rates (Murota et al., 2016). It is natural therefore to extend the DSF model with an explicit kinetic term for reversible sorption, to complement the existing kinetic fixation term, and to see the effect of different sorption rates to binding sites on the depth profile results.

This paper sets out a modified-Diffusion-Sorption-Fixation (mDSF) model where the sorption kinetics for both reversible and irreversible fixation are treated explicitly as pseudo-first order chemical reactions. A second modification is the inclusion of an advection term for the transport of radiocesium in migrating pore water. Using generic input parameters from the literature, we test the mDSF model for reproducing radiocesium depth profiles measured in Fukushima soils. The mDSF equations are solved numerically using the finite element method for spatial discretization, and the finite difference method for temporal discretization. The model is able to successfully reproduce the exponential-shape profiles with long-tails at large depths. The scope of the model is assessed by varying the input parameters within their plausible ranges. This process establishes the key parameters and their effect on the results. Finally we explore input parameters which yield radiocesium distributions displaying a peak in activity below the ground surface.

2. Methods

2.1 Model

Radiocesium can be in one of three states in the mDSF model. Mobile radiocesium is defined as the fraction that can migrate through pores in the dissolved form. Sorbed

radiocesium is the fraction that is reversibly bound to soil. Fixed radiocesium is irreversibly attached to soil.

The mDSF model couples the advection dispersion equation with a fully kinetic reversible/irreversible model of sorption. Figure 1(a) depicts the various quantities within the soil-water-air mixture, and Fig. 1(b) gives a schematic of the processes captured by the model. The radiocesium inventory obeys a mass balance equation as follows:

$$\frac{\partial A}{\partial t} + v \frac{\partial C_w}{\partial z} - D_e \frac{\partial^2 C_w}{\partial z^2} = -\lambda A, \quad (1)$$

where A (Bq m^{-3}) is the total radiocesium concentration per unit in situ volume. A is a function of the time following fallout deposition, t (s), and the depth coordinate, z (m). The parameter v (m s^{-1}) is the Darcy velocity in z -direction, C_w (Bq m^{-3}) is the mobile (dissolved) radiocesium concentration per unit volume of water, D_e ($\text{m}^2 \text{s}^{-1}$) is the effective dispersion coefficient for the dissolved radiocesium in the soil pores, and λ (s^{-1}) is the radioactive decay constant. The total radiocesium concentration A is

$$A = \varepsilon S_r C_w + \rho_d (C_{sr} + C_{si}), \quad (2)$$

where ε (-) is the soil porosity, S_r (-) is degree of water saturation of the pores, ρ_d (kg m^{-3}) is dry soil density, C_{sr} (Bq kg^{-1}) is the concentration of reversibly sorbed radiocesium per unit mass of soil and C_{si} (Bq kg^{-1}) is the concentration of irreversibly bound radiocesium per unit mass of soil.

Kinetic sorption and fixation are assumed to be pseudo-first order chemical reactions. The governing equations for the sorbed (reversible) fraction and fixed (irreversible) fraction are

$$\frac{\partial C_{sr}}{\partial t} = k_r (K_r C_w - C_{sr}) - \lambda C_{sr}, \quad (3)$$

$$k_r = \begin{cases} k_{rs} & \text{if } K_r C_w \geq C_{sr} \\ k_{rd} & \text{if } K_r C_w < C_{sr} \end{cases},$$

$$\frac{\partial C_{si}}{\partial t} = k_i (K_i C_w - C_{si}) - \lambda C_{si}, \quad (4)$$

$$k_i = \begin{cases} k_{is} & \text{if } K_i C_w \geq C_{si} \\ 0 & \text{if } K_i C_w < C_{si} \end{cases},$$

where K_r and K_i ($\text{m}^3 \text{kg}^{-1}$) are distribution coefficients for sorbed and fixed radiocesium, k_{rs} and k_{rd} (s^{-1}) are kinetic rates for sorption and desorption, respectively, between sorbed and mobile radiocesium, and k_{is} (s^{-1}) is fixation rate from mobile to irreversibly bound radiocesium. These kinetic formulae are the same as those used in models by Onishi and Perkins (1994) and Fiengo Perez et al. (2015). Although in reality sorption and desorption rates depend on the ion concentration, the model does not account for this, as radiocesium concentrations in fallout-contaminated environments are typically much lower than in laboratory tests.

Substituting Eq. (2), Eq. (3) and Eq. (4) into Eq. (1) yields

$$\varepsilon S_r \frac{\partial C_w}{\partial t} = -v \frac{\partial C_w}{\partial z} + D_e \frac{\partial^2 C_w}{\partial z^2} - \rho_d k_r (K_r C_w - C_{sr}) - \rho_d k_i (K_i C_w - C_{si}) - \lambda \varepsilon S_r C_w. \quad (5)$$

The model was solved numerically as follows. Equation (5) was spatially discretized and solved by the finite element method, while Eq. (3), (4) and (5) were temporally discretized and solved with the finite difference method. The spatial grid size was 0.001 m and the time increment depended on time elapsed. Initially the increment was 1 s, and this gradually

increased to 10^6 s.

2.2 Model reference parameters

Table 2 lists the input parameters in the mDSF model and their values taken for the reference case. The distribution coefficients for the sorbed and bound fractions were estimated from Sato (2015) and Tsukada et al. (2008). Sato (2015) reported total distribution coefficients for radiocesium in Fukushima samples between $2\text{--}100\text{ m}^3\text{ kg}^{-1}$. To separate the total distribution coefficient into components for reversible sorption and fixation, we considered measurements by Tsukada et al. (2008) for the exchangeable and fixed fractions of global weapons-testing ^{137}Cs and stable cesium in Japanese soil. They reported the relative amount of exchangeable to nonexchangeable ^{137}Cs of approximately 30:70. The corresponding result for stable cesium was about 10:90. The latter figure was considered to be the terminal ratio for ^{137}Cs in the long-term when equilibrium is attained (Tsukada et al., 2008). Combining these results, we estimated that K_r is $1.0\text{ m}^3\text{ kg}^{-1}$ and K_i is $9.0\text{ m}^3\text{ kg}^{-1}$. Therefore the total K_d is $10\text{ m}^3\text{ kg}^{-1}$ and the ratio of exchangeable and nonexchangeable fractions is 10:90.

The kinetic rates were also estimated from literature. With respect to the kinetic rate for the reversibly sorbed fraction, Liu et al. (1995) reported $0.01\text{--}0.03\text{ min}^{-1}$ ($1.7\times 10^{-4}\text{--}5\times 10^{-4}\text{ s}^{-1}$) for two types of soils in Taiwan based on laboratory batch tests. For the kinetic rate for the irreversibly bound fraction, IAEA (2009) cited $1.4\times 10^{-3}\text{--}1.6\text{ d}^{-1}$ ($1.6\times 10^{-8}\text{--}1.9\times 10^{-5}\text{ s}^{-1}$). Fiengo Perez et al. (2015) reported about $2\times 10^{-5}\text{ s}^{-1}$ for the sorption rate and $1\times 10^{-8}\text{ s}^{-1}$ for desorption for sediments sampled from a river in Belgium. Murota et al. (2016), assuming three sites, reported desorption rates as 8.8×10^{-4} , 6.2×10^{-2} , and $3.9\times 10^{-1}\text{ d}^{-1}$, respectively (1×10^{-8} , 7×10^{-7} , $4.5\times 10^{-6}\text{ s}^{-1}$). Considering these results, we initialized the sorption rate to the sorbed fraction

as $k_{rs}=1\times 10^{-6} \text{ s}^{-1}$, the desorption rate from the sorbed fraction $k_{rd}=1\times 10^{-8} \text{ s}^{-1}$, and the fixation rate to the bound fraction as $k_{is}=2\times 10^{-8} \text{ s}^{-1}$.

The porosity, degree of pore saturation and soil dry density were assumed to be 0.5, 0.8 and 950 kg m^{-3} , respectively. The Darcy velocity was estimated to be $2\times 10^{-8} \text{ m s}^{-1}$, based on 50% of the 1260 mm y^{-1} annual rainfall in Fukushima Prefecture penetrating into soil.

The effective dispersion coefficient in this model, D_e , applies to the transport of dissolved radiocesium through the soil. It depends primarily on the water flow velocity through the soil matrix, but also on the soil saturation and the soil particle size. It has a lower bound set by the diffusivity of Cs^+ ions in aqueous solution, $\sim 2.10\times 10^{-9} \text{ m}^2 \text{ s}^{-1}$ (Friedman and Kennedy, 1955; Sato et al. 1996). D_e is typically measured experimentally or tuned such that results of solute distribution models match field observations. Here we initially set $D_e=5.0\times 10^{-8} \text{ m}^2 \text{ s}^{-1}$, such that the model with parameters as Table 2 yields depth profiles consistent with measurements in Fukushima Prefecture. Note $5.0\times 10^{-8} \text{ m}^2 \text{ s}^{-1}$ is at the higher end of values observed in experiments on partially saturated soil with pore flow velocity equal to the Darcy velocity $v=2\times 10^{-8} \text{ m s}^{-1}$ (Beven et al., 1993). The consequences of this assumption and the other choices for the input parameters are assessed by exploring the effect of the parameters on the output results (parameter exploration).

2.3 Comparison of mDSF results with field measurements and other model results

We drew upon previously published measurements of radiocesium depth profiles within Fukushima Prefecture, Japan, to assess the mDSF model. The data are publicly available online (JAEA, 2016) and described in Matsuda et al. (2015). In summary, soil samples were collected from flat, open locations away from tall vegetation and man-made infrastructure. Layers were collected at fixed depth intervals from the surface using a scraper plate apparatus.

The in-situ mass and volume of the layers were noted, before the samples sent for drying and HPGe analysis to measure ^{137}Cs content. The layer activities (Bq m^{-3}) were normalized by the total inventories (Bq m^{-2}) for comparison with the mDSF model results. We compared the mDSF results to the measured depth profiles from the grounds of Futase Community Hall (37.31102,140.48491), 12 km south-east of Koriyama City, taken over a 4.5 y period following March 2011.

To contextualize the mDSF model results, we also report corresponding results for the simple diffusion model and the original DSF model. The formulae of these models are given in Appendices A and B, along with details for how the solutions of the formulae were obtained. For the simple diffusion model, we assumed a total dispersion coefficient of $K_d=10.0 \text{ m}^3 \text{ kg}^{-1}$, based on K_r and K_i of the mDSF reference case (Table 2). Other input parameters to the simple diffusion model were identical to the applicable mDSF reference case parameters.

For the DSF model, we set $k=2.2 \times 10^{-5} \text{ s}^{-1}$ and $D_e=5.0 \times 10^{-9} \text{ m}^2 \text{ s}^{-1}$ to yield a good fit between the DSF model results and the depth profile measured for Futase Community Hall on 7th September 2015. All other relevant parameters (K_r , ε , S_r and ρ_d) were the same as the mDSF reference case. Thus, the DSF diffusion length was $L_D=0.024 \text{ m}$ and the effective fixation rate was $k_{eff} = 8.0 \times 10^{-4} \text{ d}^{-1}$. These values are of similar magnitude to the original parameters used by Toso and Velasco (2001). The quality of the fit between the various physiochemical models and the measured depth profiles was quantified by calculating the coefficient of determination (R^2).

2.4 Parameter exploration

To evaluate the important input parameters in the mDSF model, we conducted a set of

analyses for the effect of the inputs on the predicted depth distributions. Seven variations of the reference case parameter set (Table 2) were devised, as listed in Table 3. The distribution coefficients K_r , K_i , the kinetic rates k_{rs} , k_{rd} , k_{is} , the effective dispersion coefficient D_e and the Darcy velocity v were varied between the cases.

The first five cases – High- K , Low- K , No Reverse, No Fixation and Reverse – focus on the sorption and desorption kinetics. In the High- K and Low- K cases, the distribution coefficients for sorption and fixation are ten times higher and lower, respectively, than the base case. The No Reverse case assumes that there are no reversible sorption sites, and thus is mathematically identical to the original DSF model. The No Fixation and Reverse cases both assume that there are no irreversible binding sites. The No Fixation case follows the initial parameter set in having different kinetic rates for sorption and desorption, while the Reverse case assumes identical kinetic rates for sorption and desorption. The effective dispersion coefficient is reduced by a factor of ten in the Low- D_e case compared to the initial parameter set. Finally to analyze the effect of the advection term in the model, the No Advection case sets the Darcy velocity to zero.

3. Results

3.1 Comparison with the measurements

Figure 2 compares the results for the simple diffusion, DSF and mDSF models with the measured depth profiles in Fukushima Prefecture. The depth profiles from the mDSF model show a steep reduction in the radiocesium activity concentration in the initial 3 cm of soil, followed by a longer tail in the distribution below. The inventory migrates slowly downwards in the soil column over the years between the sampling campaigns. The mDSF model results fit the environmental measurements best for the 1st sampling campaign ($R^2=0.96$). The mDSF

results show larger deviations from the measurements for the later campaigns (lowest R^2 is 0.83).

The results from the simple diffusion model all have Gaussian-shapes, which do not fit the measured profiles particularly well. The original DSF model results also have Gaussian-shape depth profiles for the early sampling periods. For the later campaigns however, the DSF depth profiles are more similar to the measured profiles. This is in part a reflection of our choice to tune the DSF model input parameters to give results that fit best to the final sampling campaign measurements. Fitting input parameters to one of the other campaigns instead would yield better results for that campaign. At long timescales, the original DSF model results will tend to an exponential-shape. Thus the model ultimately will not fit mature depth profiles measured in the field that display a long-tail exponential shape (Antonopoulos-Domis et al., 1995).

In the mDSF model, the fraction of reversibly bound radiocesium decreases monotonically over time, while the irreversibly bound fraction increases monotonically (Figure 3). The competition between the states is highest in the initial few years following the fallout. The ratio between reversible and irreversible fractions approaches the equilibrium ratio of 10:90 (set by $K_r:K_i$) around six years following fallout. This tendency is consistent with the measurements by Tsukada et al. (2008), although the equilibrium state is reached faster in the mDSF model results.

3.2 Parameter exploration

We investigated the scope of the depth profile results from the mDSF model by varying the input parameters (Table 3 and Figure 4). The distribution coefficient K affects the slope of the depth profile (cf. the High- K – crosses, reference – filled circles, and Low- K – open

circles, cases in Fig. 4(a)). High distribution coefficients promote radiocesium binding to soil, thus inhibiting downward radiocesium migration in the dissolved fraction.

Lowering the effective dispersion coefficient (Low- D_e case – triangle markers in Fig. 4(a)) reduces the rate of downward migration of the dissolved fraction. This has a similar effect to increasing the distribution coefficient. The results of the Low- D_e and High- K cases, where the effective dispersion coefficient and the distribution coefficients are lowered and increased, respectively, by a factor of 10, coincide on Fig. 4(a). This indicates that dispersion is the dominant mechanism behind downward migration of the dissolved fraction in the model. This observation is confirmed by the No Advection case (Fig. 4(a) – plus markers), which coincides with the results of the reference case. Although advection is an insignificant process in the model for radiocesium migration, the effective dispersion coefficient D_e depends on the Darcy flow velocity v . Therefore rainfall primarily affects the radiocesium distribution via dispersive rather than advective flows through the soil pores.

The depth distribution at the terminal state in the original DSF model is determined by an effective diffusion length (Antonopoulos-Domis et al., 1995; Toso and Velasco, 2001). The equivalent parameter for the mDSF model is

$$L_d = \sqrt{\frac{D_e}{\rho_d(k_r K_r + k_i K_i)}} \quad (6)$$

L_d contains the key parameters in the model affecting the downward migration of radiocesium. In Fig. 4(b) we show the results of the parameter exploration where the depth axis z is normalized by this effective diffusion length. Normalization results in the overlap of the reference, High- K , Low- K , Low- D_e and No Advection cases (Fig. 4(b)).

The remaining cases in Figure 4 are the No Reverse, Reverse and No Fixation. The No

Reverse case (Fig. 4, open diamonds) results in a distribution with an exponential shape. This exponential distribution is the terminal state, and thus no further migration happens, as is the case with the original DSF model. The depth distribution of the No Reverse case coincides with the ‘initial exponential’ black line in in Fig. 4(b), which shows the analytical distribution

$$C = C_0 \exp\left(-\frac{\rho_t z}{\beta_0}\right) = C_0 \exp\left(-\frac{z}{L_d}\right), \quad (7)$$

where C_0 is the radiocesium concentration at the surface, ρ_t (kg m^{-3}) is the wet, in-situ, soil density and β_0 (kg m^{-2}) is the relaxation mass.

The radiocesium distribution of the No Fixation case (Fig. 4, filled squares) can be separated into two parts. Initially there is an exponential-shape distribution below the ground surface. In deeper regions, the depth profile takes on a Gaussian shape. This profile is a result of net desorption occurring in the shallow region, while net sorption occurs beneath. The difference in kinetic rates of sorption and desorption result in this shape of depth distribution.

In case of the Reverse parameter set, the sorption and desorption rates are identical. This results in migration dynamics the same as in the simple diffusion model. Thus a Gaussian-shape depth distribution results (Fig. 4, asterisk markers).

4. Discussion

4.1 Depth distribution stages following fallout

The mDSF depth profiles can be divided into three stages: the initial Gaussian stage, the exponential stage and the migration stage (Figure 5). These stages correspond to competition between the various processes affecting radiocesium migration and binding. In the initial

Gaussian stage dispersion is the dominant process. In the exponential stage, dispersion and sorption are main processes. In the migration stage, desorption at shallow depths below the surface and sorption (both reversible and fixation) deeper beneath happen simultaneously. The initial Gaussian stage is very short, lasting less than 50 minutes in the reference simulation case. Thus, the radiocesium distribution becomes an exponential shape promptly after the fallout.

The exponential stage lasts for around a month in the reference case. The kinetics of sorption to both reversible and irreversible sites give rise to the initial exponential shape. International Commission on Radiation Units and Measurements (1994) summarized research showing that the relaxation mass depth of the initial exponential distribution varies between 0.1-2.0 g cm⁻² in samples measured 3-4 weeks after the Chernobyl accident. Malins et al. (2016) suggested a range of relaxation mass depths between 0.5-1.2 g cm⁻² is at two months after the Fukushima accident. In our model, initial relaxation mass for the reference case can be determined by

$$\beta_0 = \rho_t L_d = (\rho_d + \varepsilon S_r \rho_w) \sqrt{\frac{D_e}{\rho_d (k_r K_r + k_i K_i)}} \approx 0.9 \text{ g cm}^{-2}, \quad (8)$$

where ρ_w is the density of water. This value is within the range of both ICRU (1994) and Malins et al. (2016). Thus, the diffusion length for the mDSF model governs the initial relaxation mass depth.

The change in shape of the depth profile over the long-term migration stage is slow. This tendency is consistent with the filed investigations such as Matsunaga et al. (2013), Nakanishi et al. (2014) and Koarashi et al. (2016). Matsunaga et al. (2013) concluded that rainfall had a limited effect on radiocesium distribution in this stage, although others have suggested that

heavy typhoon rains is a factor behind the faster migration of radiocesium in soil in Fukushima Prefecture than in Eastern Europe after the Chernobyl accident (Konoplev et al., 2016). The mDSF model suggests that the early depth profiles in the initial Gaussian and exponential stages are affected by rainfall intensity through the dispersion coefficient D_e . A limitation of the model is that D_e is based on yearly average Darcy velocity data, so cannot capture the highly variable temporal and spatial characteristics of rainfall within this early period (Lacey et al., 2016). However, these short term rainfall fluctuations will have a little bearing on the evolution of the depth profile in the migration stage which proceeds on the timescale of years.

4.2 Long tails

Antonopoulos-Domis et al. (1995) reported two exponential characteristics of Chernobyl fallout within soil. A similar tendency has been observed with Fukushima fallout (e.g., Matsuda et al., 2015; Takahashi et al., 2015). An example of such a depth profile in Fukushima Prefecture is shown in Figure 6(a) (Matsuda et al., 2015). The Antonopoulos-Domis et al. (1995) model reproduces the long tails through an advection term. However, this requires a higher advective flow velocity in the model than is reasonable in reality.

In the mDSF model, long tails are expressed without considering such a high Darcy velocity, for example Fig. 2 (reference case) and Fig. 4 (No Advection case). Figure 7 shows the breakdown of the radiocesium concentration into reversibly and irreversibly sorbed fractions at $t = 275$ d for the reference case. The figure also shows the apparent distribution coefficient which is defined as $K_a = C_{sr}/C_{sw}$. The long tail of the depth distribution is a feature of the crossover between predominantly sorbed radiocesium near the surface, and

predominantly fixed radiocesium at larger depths. In the shallow region ($z < 3$ cm), the apparent distribution coefficient is higher than the $1.0 \text{ m}^3 \text{ kg}^{-1}$ parameter value applied for K_r (Table 2). Thus desorption from the reversible binding site is occurring in this region. On the other hand, in the deeper region, the apparent distribution coefficient is slightly less than $1.0 \text{ m}^3 \text{ kg}^{-1}$, meaning net sorption is occurring. If the kinetic rates of sorption and desorption are identical, the mDSF model does not predict a long tail in the distribution (cf. Reverse case in Fig. 4). Therefore, different rates of kinetic sorption and desorption give rise to the long tail in the depth distribution.

4.3 Peak in activity concentration beneath the ground surface

Depth distributions with a peak below the ground surface (Fig. 6(b)) are sometimes seen in soils contaminated with fallout (Matsuda et al., 2015). The mDSF model can yield such distributions if the effective dispersion and distribution coefficients are set to be much smaller than those of the reference case (Fig. 8(a)). The effect of this change is to increase the relative importance of advection for radiocesium redistribution within the soil. However, the values of K and D_e employed in Fig. 8(a) are not reflective of the reality for radiocesium contaminated soil.

We therefore considered the effect of varying K with depth, which may occur, for instance, if soil has high organic matter content near the surface (e.g., Matsunaga et al., 2013; Koarashi et al., 2016). High organic matter content corresponds to low K , as radiocesium has less affinity for sorbing to the soil. We calculated the depth profile assuming K linear increases with depth down to $z=0.01$ m, i.e. $K_r=100z \text{ m}^3 \text{ kg}^{-1}$ and $K_i=900z \text{ m}^3 \text{ kg}^{-1}$. The values of K were as per Table 2 for $z > 0.01$ m. This gives rise to the depth distributions shown in Fig. 8(b). These distributions show the characteristic peak in the activity concentration below

the ground surface seen at some fallout contaminated sites. Profiles with this shape can be fitted with a hyperbolic secant distribution (Matsuda et al., 2015). Thus, the results suggest that depth dependency of the distribution coefficient can give rise to a distribution with a peak under the surface. This hypothesis could be checked with laboratory experiments.

5. Conclusions

In this paper, we proposed a modified Diffusion-Sorption-Fixation (mDSF) model for the migration of radiocesium fallout with depth in soil. The original DSF model was expanded by adding kinetics for reversible sites. The mDSF model can reproduce the exponential depth distribution of radiocesium seen initially following fallout in Fukushima soils. The distribution is created promptly after fallout, followed by slow migration deeper underground over time. The relaxation mass depth of the initial exponential distribution is determined by the diffusion length, which depends on the distribution coefficient, sorption rate and effective dispersion coefficient.

A key feature of the mDSF model is the ability to reproduce long tails in the radiocesium depth distribution at large depths below the surface. These tails are caused by differing rates of kinetic sorption and desorption in the model, primarily affecting the distribution of the reversibility sorbed radiocesium fraction with depth.

Depth distributions showing a peak in activity concentration beneath the surface can be explained by setting lower K values for the surface soil. This could be caused, for instance, by high organic matter content at the surface.

The model thus offers a physical basis for the types of radiocesium depth profiles observed in contaminated environments. It should be noted, however, that migration is controlled not only by the processes captured by the mDSF model, but also by other

mechanical processes including bioturbation, erosion/sedimentation, frost heaving and thawing, and colloid migration (e.g., Miyahara et al., 2015; Konoplev et al., 2016). Further laboratory and field survey investigations could ascertain the importance of these processes to the migration of radiocesium fallout within soil.

Acknowledgments

The authors would like to appreciate the reviewers and editors for their comments and suggestions on the manuscript. The authors thank Drs. Masahiko Machida, Norihiro Matsuda and Kaname Miyahara of JAEA for the useful discussions.

Appendix A: Formulae of simple diffusion model

The simple diffusion model is a limited case of the mass balance equations (1) and (2) in the main text. There is no advective transport ($v=0$) and a single reversible binding site (i.e. $C_{si}=0$). The bound radiocesium is assumed to be in instantaneous equilibrium with the mobile fraction:

$$C_{sr} = K_d C_w. \quad (\text{A.1})$$

Note the total distribution coefficient K_d is used here instead of K_r as there is a single sorption site only. Combining equations (1), (2) and (A.1) yields

$$\frac{\partial C_w}{\partial t} = D_a \frac{\partial^2 C_w}{\partial z^2} - \lambda C_w, \quad (\text{A.2})$$

where $D_a = \frac{D_e}{\varepsilon S_r + \rho_d K_d}$. The analytical solution for equation (A.2) given a pulse-like input of fallout at $t=0$ is

$$C_w = \frac{Q_0}{2\sqrt{\pi D_a t}} \exp\left(-\frac{z^2}{4D_a t}\right) \exp(-\lambda t), \quad (\text{A.3})$$

where Q_0 (Bq m⁻²) is a constant determined by the initial fallout activity per unit area.

Appendix B: Formulae of the DSF model

The DSF model also is a derived case of the mass balance equations (1) and (2) in the main text. The DSF model has no advection term ($v=0$) and two binding sites: reversible and irreversible. The reversible site is assumed to be in instantaneous equilibrium with the dissolved fraction:

$$C_{sr} = K_r C_w. \quad (\text{A.4})$$

The kinetic term for the irreversible fraction is:

$$\rho_d \frac{\partial C_{si}}{\partial t} = \varepsilon S_r k C_w - \lambda \rho_d C_{si} = k_{eff} (\varepsilon S_r + \rho_d K_r) C_w - \lambda \rho_d C_{si}, \quad (\text{A.5})$$

where k (s^{-1}) is the fixation rate to the irreversible binding site and $k_{eff} = \frac{k}{1 + \rho_d K_r / \varepsilon S_r}$.

There is an analytical solution of Equation (A.7) for the dissolved and reversibly sorbed components of the radiocesium inventory, given a single pulse input of fallout at $t=0$ (set by activity constant Q_0 ($Bq\ m^{-2}$)):

$$f = \frac{Q_0}{\sqrt{\pi k_{eff} t L_D}} \exp\left(-\frac{z^2}{4L_D k_{eff} t}\right) \exp(-k_{eff} t) \exp(-\lambda t), \quad (A.6)$$

where $f = \varepsilon S_r C_w + \rho_d C_{sr} = (\varepsilon S_r + \rho_d K_r) C_w$ and L_D (m) is the diffusion length given by $L_D = \sqrt{D_e / \varepsilon S_r k}$.

The irreversibly bound fraction is given by numerical integrating the following equation using the finite difference method:

$$C_{si} = \frac{k_{eff}}{\rho_d} \exp(-\lambda t) \int_t^0 f(z, t') dt' \quad (A.7)$$

References

- Antonopoulos-Domis, M., Clouvas, A., Hiladakis, A., Kadi, S., 1995. Radiocesium distribution in undisturbed soil: measurements and diffusion-advection model. *Health Phys.* 69, 949-953.
- Beck, H.L., 1966. Environmental Gamma Radiation from Deposited Fission Products, 1960-1964. *Health Phys.* 12, 313-322.
- Beresford, N.A., Howard, B.J., Barnett, C.L., Crout, N.M.J., 1992. The uptake by vegetation of Chernobyl and aged radiocaesium in upland West Cumbria. *J. Environ. Radioact.* 16, 181-195. doi:10.1016/0265-931X(92)90015-L
- Beven, K.J., Henderson, D.E., Reeves, A., 1993. Dispersion parameters for undisturbed partially saturated soil. *J. Hydrol.* 143, 19-43. DOI:10.1016/0022-1694(93)90087-P
- Bossew, P. and Kirchner, G., 2004. Modelling the vertical distribution of radionuclides in soil. Part 1: the convection – dispersion equation revisited, *J. Environ. Radioact.* 73, 127-150. doi: 10.1016/j.jenvrad.2003.08.006
- Clouvas, A., Xanthos, S., Kadi, S., Antonopoulos-Domis, M., 2013. Measurements and modelling of ^{137}Cs distribution on ground due to the Chernobyl accident: a 27-y follow-up study in northern Greece. *Radiat. Prot. Dosim.* 160, 293-296. doi:10.1093/rpd/nct302
- Evrard, O., Laceby, J., Lepage, H., Onda, Y., Cerdan, O., Ayrault, S., 2015. Radiocesium transfer from hillslopes to the Pacific Ocean after the Fukushima Nuclear Power Plant accident: A review. *J. Environ. Radioact.* 148, 92-110. doi: 10.1016/j.jenvrad.2015.06.018
- Fiengo Perez, F., Sweeck, L., Bauwens, W., Van Hees, M., Elskens, M., 2015. Adsorption and desorption kinetics of ^{60}Co and ^{137}Cs in fresh water rivers. *J. Environ. Radioact.* 149, 81-89. doi:10.1016/j.jenvrad.2015.07.010

- Friedman, A.M. and Kennedy, J.W., 1955. The self-diffusion coefficients of potassium, cesium, iodide and chloride ions in aqueous solutions. *J. Am. Chem. Soc.* 77, 4499-4501. doi:10.1021/ja01622a016
- Fuller, A.J., Shaw, S., Ward, M.B., Haigh, S.J., Mosselmans, J.F.W., Peacock, C.L., Stackhouse, S., Dent, A.J., Trivedi, D., Burke, I.T., 2015. Caesium incorporation and retention in illite interlayers. *Appl. Clay Sci.* 108, 128-134. doi:10.1016/j.clay.2015.02.008
- Gale, H.J., Humphreys, D.L.O., Fisher, E.M.R., 1964 Weathering of Caesium-137 in Soil. *Nature* 201, 257-261. doi:10.1038/201257a0
- He, Q. and Walling, D., 1997. The distribution of fallout ¹³⁷Cs and ²¹⁰Pb in undisturbed and cultivated soils. *Appl. Radiat. Isot.* 48, 677-690. doi:10.1016/S0969-8043(96)00302-8
- Hillmann, U., Schimmack, W., Jacob, P., Bunzl, K., 1996. In situ γ -spectrometry several years after deposition of radiocesium. Part I. Approximation of depth distributions by the Lorentz function. *Radiat. Environ. Biophys.* 35, 297-303.
- International Atomic Energy Agency, 2009. Quantification of radionuclide transfer in terrestrial and freshwater environments for radiological assessments. IAEA-TECDOC-1616, Vienna. (accessed 29.07.16) at http://www-pub.iaea.org/MTCD/publications/PDF/te_1616_web.pdf
- International Commission on Radiation Units and Measurements, 1994. Gamma-ray spectrometry in the environment. ICRU Report 53.
- JAEA, 2016. Database for Radioactive Substance Monitoring Data - Depth Distribution in Soil. URL: <http://emdb.jaea.go.jp/emdb/en/>. Date (accessed 05.10.16.)
- Kirchner, G., 1998. Applicability of compartmental models for simulating the transport of radionuclides in soil. *J. Environ. Radioact.* 38, 339-352. doi:10.1016/S0265-931X(97)00035-0

- Konoplev, A., Golosov, V., Laptev, G., Nanba, K., Onda, Y., Takase, T., Wakiyama, Y., Yoshimura, K., 2016. Behavior of accidentally released radiocesium in soil-water environment: Looking at Fukushima from a Chernobyl perspective. *J. Environ. Radioact.* 151, 568-578. doi: 10.1016/j.jenvrad.2015.06.019
- Koarashi, J., Nishimura, S., Nakanishi, T. Atarashi-Adnoh, M., Takeuchi, E., Muto, K., 2016. Post-deposition early-phase migration and retention behavior of radiocesium in a litter–mineral soil system in a Japanese deciduous forest affected by the Fukushima nuclear accident. *Chemosphere* 165, 335-341. doi:10.1016/j.chemosphere.2016.09.043
- Krouglov, S.V., Filipas, A.S., Alexakhin, R.M., Arkhipov, N.P., 1996. Long-term study on the transfer of ^{137}Cs and ^{90}Sr from Chernobyl-contaminated soils to grain crops. *J. Environ. Radioact.* 34, 267-286. doi:10.1016/0265-931X(96)00043-4
- Lacey, J.P., Chartin, C., Evrard, O., Onda, Y., Garcia-Sanchez, L., Cerdan, O., 2016. Rainfall erosivity in catchments contaminated with fallout from the Fukushima Daiichi nuclear power plant accident. *Hydrol. Earth Syst. Sci.* 20, 2467-2482. doi:10.5194/hess-20-2467-2016
- Liu, D., Hsu, C., Chuang, C., 1995. Ion-exchange and sorption kinetics of cesium and strontium in soils. *Appl. Radiat. Isot.* 46, 839-846. doi:10.1016/0969-8043(95)00175-D
- Malins, A., Kurikami, H., Nakama, S., Saito, T., Okumura, M., Machida, M., Kitamura, A., 2016. Evaluation of ambient dose equivalent rates influenced by vertical and horizontal distribution of radioactive cesium in soil in Fukushima Prefecture. *J. Environ. Radioact.* 151, 38-49. doi:10.1016/j.jenvrad.2015.09.014
- Matsuda, N., Mikami, S., Shimoura, S., Takahashi, J., Nakano, M., Shimada, K., Uno, K., Hagiwara, S., Saito, K., 2015. Depth profiles of radioactive cesium in soil using a scraper plate over a wide area surrounding the Fukushima Dai-ichi Nuclear Power Plant, Japan. *J. Environ. Radioact.* 139 427-434. doi:10.1016/j.jenvrad.2014.10.001

- Matsunaga, T., Koarashi, J., Atarashi-Andoh, M., Nagao, S., Sato, T., Nagai, H., 2013. Comparison of the vertical distributions of Fukushima nuclear accident radiocesium in soil before and after the first rainy season, with physicochemical and mineralogical interpretations. *Sci. Total Environ.* 447, 301-314. doi: 10.1016/j.scitotenv.2012.12.087
- Mikami, S., Maeyama, T., Hoshide, Y., Sakamoto, R., Sato, S., Okuda, N., Demongeot, S., Gurriaran, R., Uwamino, Y., Kato, H., Fujiwara, M., Sato, T., Takemiya, H., Saito, K., 2015. Spatial distributions of radionuclides deposited onto ground soil around the Fukushima Dai-ichi Nuclear Power Plant and their temporal change until December 2012. *J. Environ. Radioact.* 139, 320-343, doi:10.1016/j.envrad.2014.09.010
- Miyahara, K., McKinley, I., Saito, K., Hardie, S., Iijima, K., 2015. Use of Knowledge and Experience Gained from the Fukushima Daiichi Nuclear Power Station Accident to Establish the Technical Basis for Strategic Off-site Response, JAEA-Review 2015-001. doi:10.11484/jaea-review-2015-001
- Mukai, H., Hatta, T., Kitazawa, H., Yamada, H., Yaida, T., Kogure, T., 2014. Speciation of radioactive soil particles in the Fukushima contaminated area by IP autoradiography and microanalyses. *Environ. Sci. Tech.* 48, 13053-13059. doi:10.1021/es502849e
- Murota, K., Saito, T., Tanaka, S., 2016. Desorption kinetics of cesium from Fukushima soils. *J. Environ. Radioact.* 153, 134-140. doi:10.1016/j.jenvrad.2015.12.013
- Nakanishi, T., Matsunaga, T., Koarashi, J., Atarashi-Andoh, M., 2014. ¹³⁷Cs vertical migration in a deciduous forest soil following the Fukushima Dai-ichi Nuclear Power Plant accident. *J. Environ. Radioact.* 128, 9-14. doi:10.1016/j.jenvrad.2013.10.019
- Ohnuki, T. and Tanaka, T., 1989. Migration of radionuclides controlled by several different migration mechanisms through a sandy soil layer. *Health Phys* 56, 47-53.
- Okumura, M., Nakamura, H., Machida, M., 2013. Mechanism of strong affinity of clay minerals to radioactive cesium: first-principles calculation study for adsorption of cesium

- at frayed edge sites in Muscovite. *J. Phys. Soc. Jpn.* 82, 033802.
doi:10.7566/jpsj.82.033802
- Onishi, Y. and Perkins, W. A., 1994. TODAM One-Dimensional Sediment and Contaminant Transport Model with Multiply Connected Networks Volume 1: Theory and Numerical Methods, Pacific Northwest National Laboratory, Richland, Washington.
- Saito, K. and Onda, Y., 2015. Outline of the national mapping projects implemented after the Fukushima accident. *J. Environ. Radioact.* 139, 240-249.
doi:10.1016/j.jenvrad.2014.10.009
- Sato, H., Yui, M., Yoshikawa, H., 1996. Ionic Diffusion Coefficients of Cs⁺, Pb²⁺, Sm³⁺, Ni²⁺, SeO₄²⁻ and TcO₄⁻ in Free Water Determined from Conductivity Measurements. *J. Nucl. Sci. Technol.* 33, 950-955. DOI: 10.1080/18811248.1996.9732037
- Sato, H., 2015. Derivation of apparent diffusion coefficient (D_a) and distribution coefficient (K_D) from evolution of depth distribution of radiocaesium in soil contaminated by the Fukushima NPP accident. Proc. 4th Int. Symp. Radiol. Issues for Fukushima's Revital. Futur. 85-91, Fukushima, Japan. (accessed 29.07.16) at http://www.rri.kyoto-u.ac.jp/anzen_kiban/outcome/Symposium'15_Proceedings_EN.pdf
- Takahashi, J., Tamura, K., Suda, T., Matsumura, R., Onda, Y., 2015. Vertical distribution and temporal changes of ¹³⁷Cs in soil profiles under various land uses after the Fukushima Dai-ichi Nuclear Power Plant accident. *J. Environ. Radioact.* 139, 351-361.
doi:10.1016/j.jenvrad.2014.07.004
- Toso, J.P. and Velasco, R.H., 2001. Describing the observed vertical transport of radiocesium in specific soils with three time-dependent models. *J. Environ. Radioact.* 53, 133-144.
doi:10.1016/S0265-931X(00)00105-3
- Tsukada, H., Takeda, A., Hisamatsu, S., Inaba, J., 2008. Concentration and specific activity of fallout ¹³⁷Cs in extracted and particle-size fractions of cultivated soils. *J. Environ.*

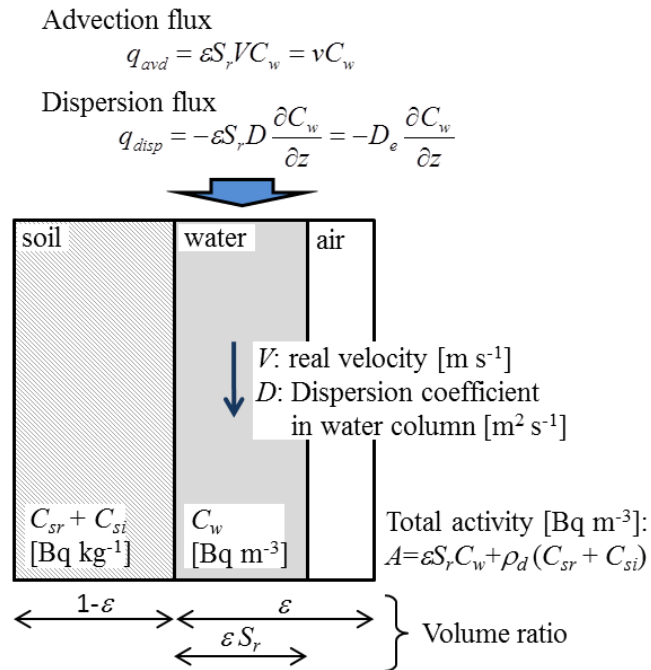
Radioact. 99, 875-881. doi:10.1016/j.jenvrad.2007.11.014

van Genuchten, M. T. and Wagenet, R. J., 1989. Two-site/two-region models for pesticide transport and degradation: theoretical development and analytical solutions. *Soil Sci. Soc. Am. J.* 53, 1303-1310.

Yesin, T. and Cakir, N., 1989. Caesium-137 and Caesium-134 levels in soil in a tea plantation in Turkey after the Chernobyl accident. *Int. J. Radiat. Appl. Instrum. Part A* 40, 209-211. doi:10.1016/0883-2889(89)90149-4

Figure 1 Schematic of the mDSF model showing (a) advection and dispersion in partially saturated soil and (b) the three states of radiocesium and the transfer pathways between the states.

(a)



(b)

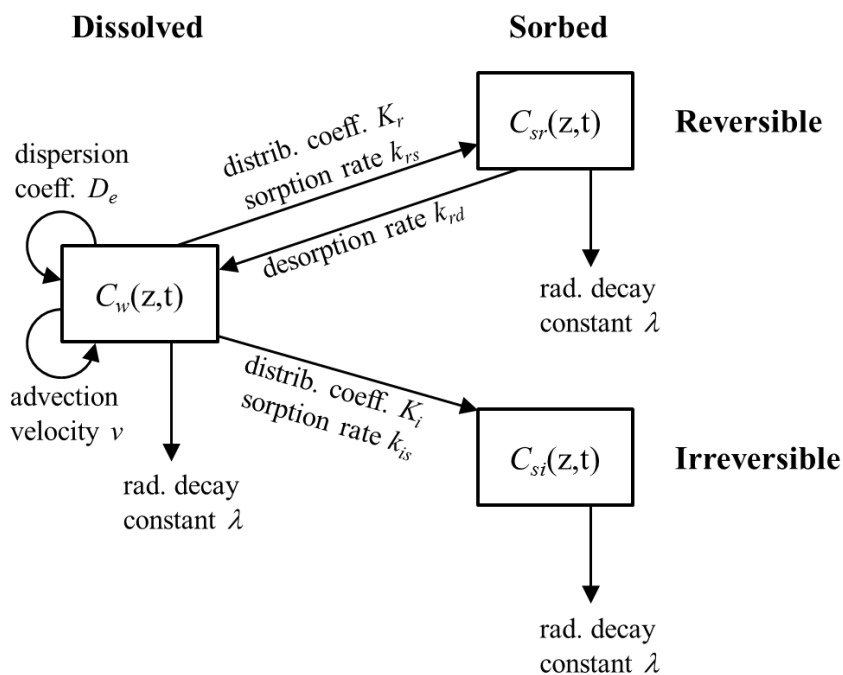


Figure 2 Radiocesium distributions from the mDSF model compared with samples taken at Futase Community Hall, on (a) 15th December 2011, (b) 30th November 2012, (c) 13th November 2013 and (d) 7th September 2015.

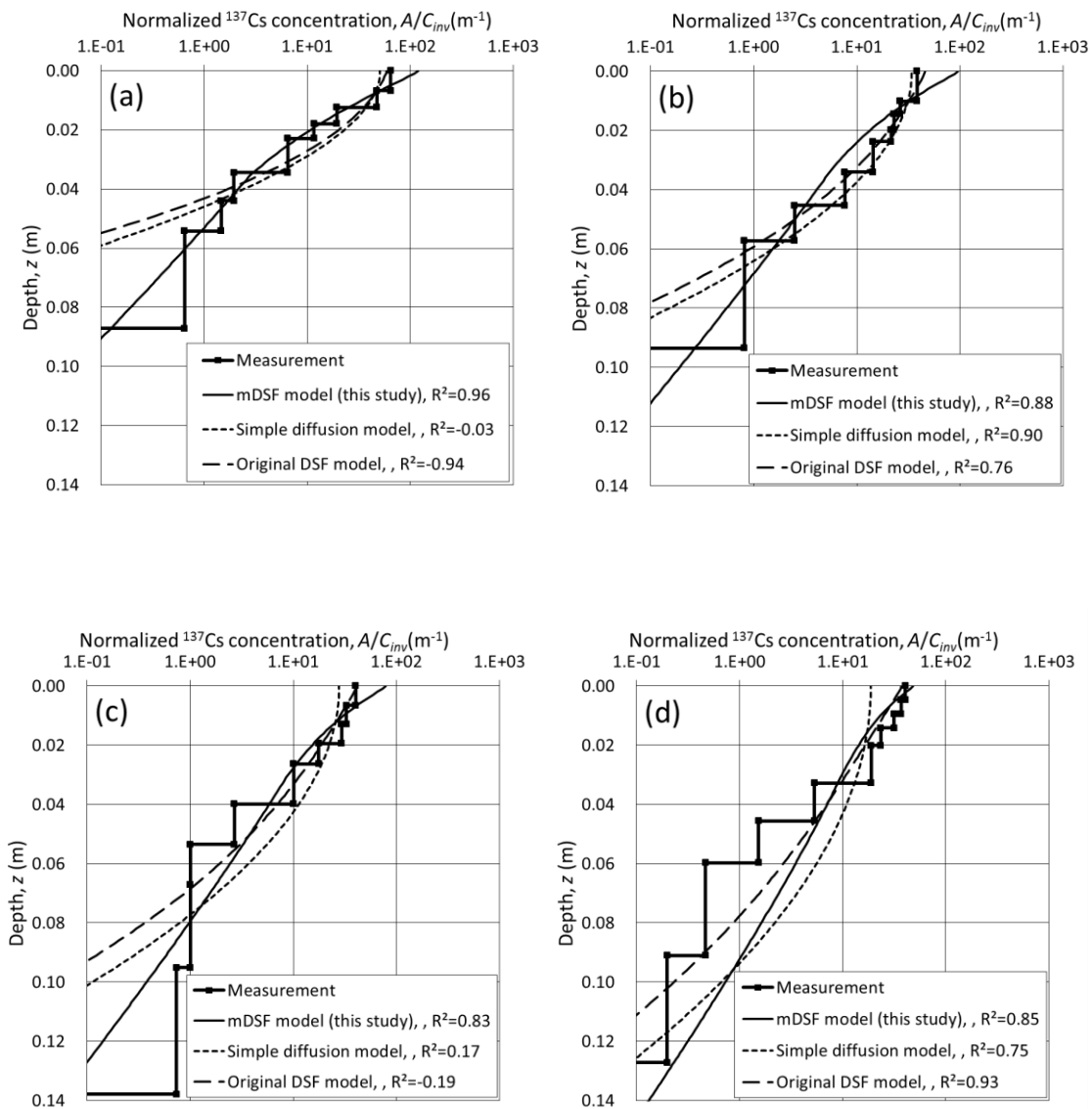


Figure 3 Fractions of reversibly and irreversibly sorbed radiocesium at 5 cm soil depth with years elapsed post-fallout.

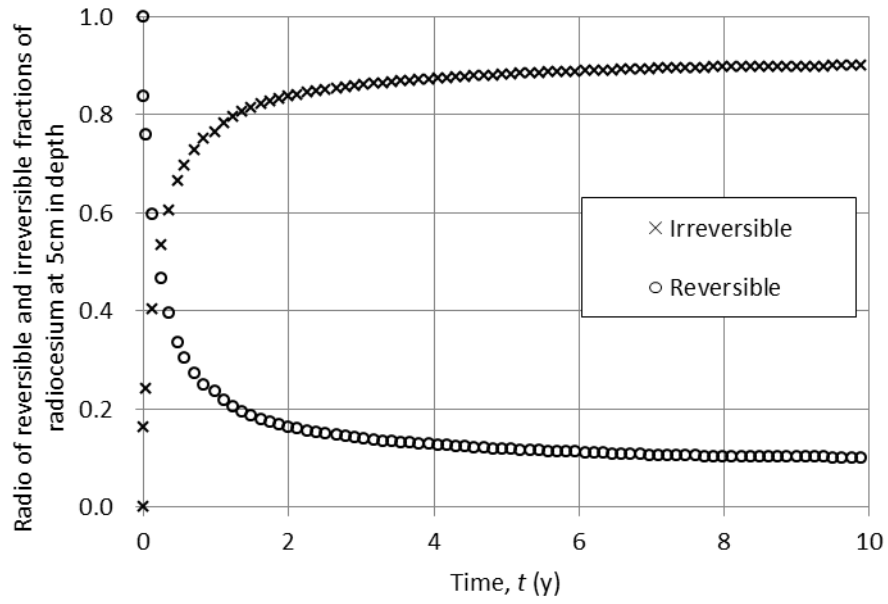
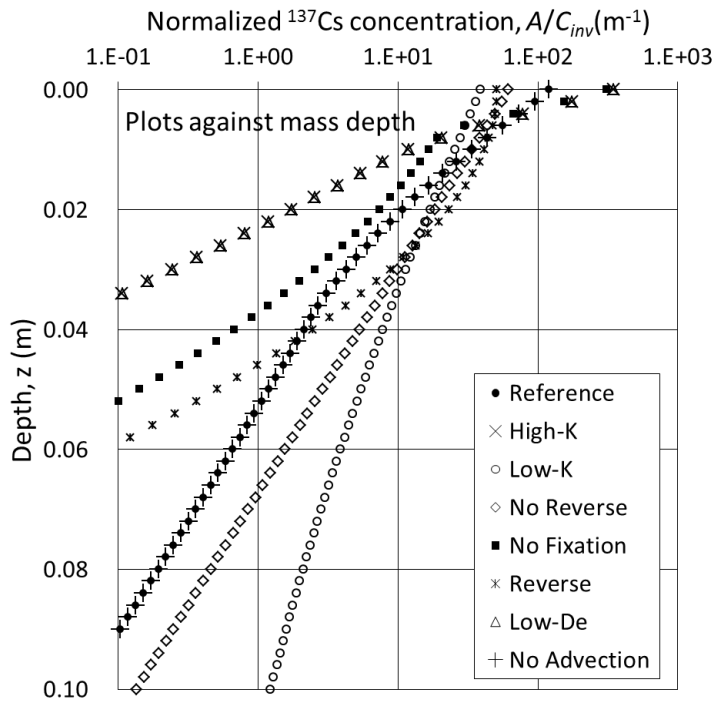


Figure 4 Results of the parameter exploration analysis. Depth distributions given by the mDSF model at 275 days post-fallout, plotted against (a) physical depth, and (b) physical depth normalized by the diffusion length, L_d .

(a)



(b)

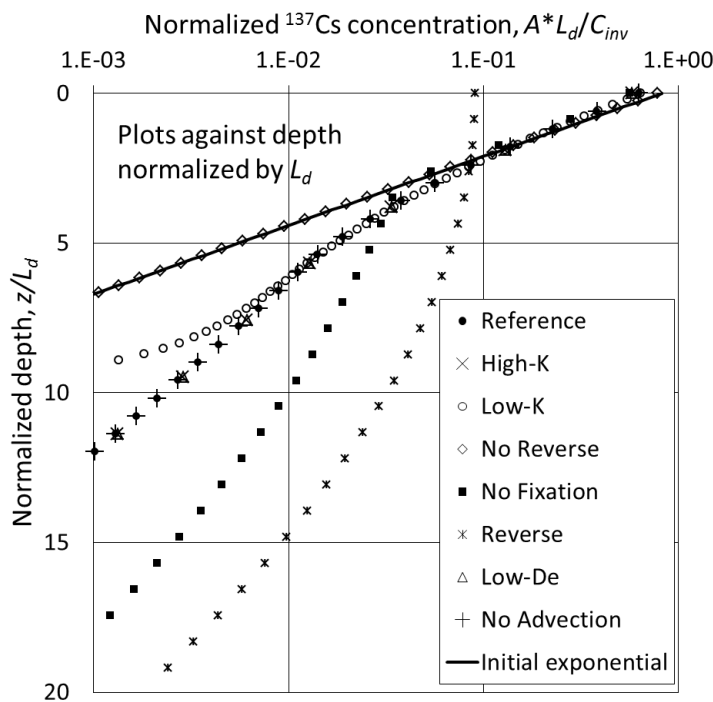


Figure 5 Radiocesium depth distributions in the early stages following fallout (mDSF results with initial parameter set).

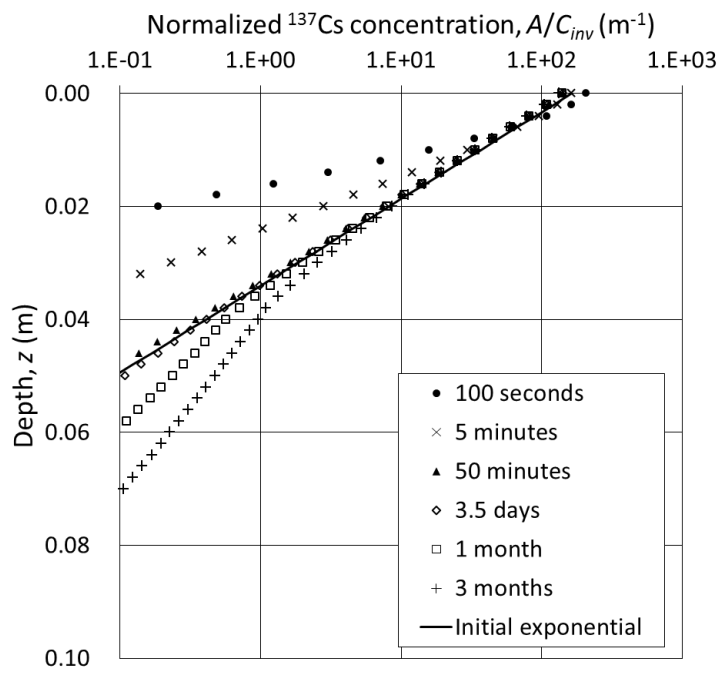
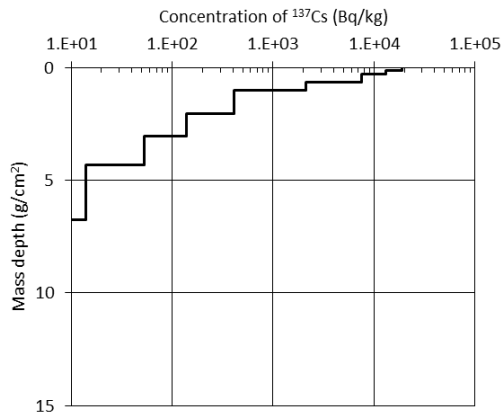


Figure 6 Two types of radiocesium depth distribution observed in Fukushima Prefecture (Matsuda et al., 2015). (a) Long tail to the distribution at large mass depths. (b) Peak in the radiocesium activity below the surface.

(a)



(b)

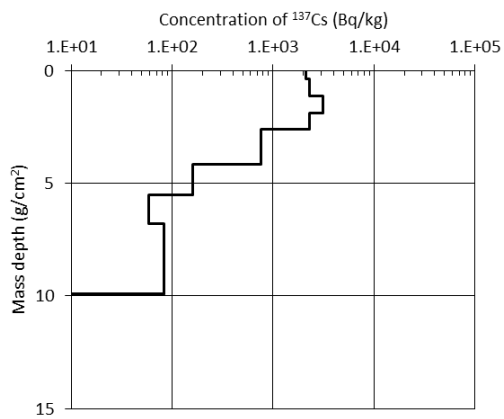


Figure 7 Breakdown of the radiocesium distribution into sorbed and bound components for the mDSF model with the initial parameter set, 275 days post-fallout. Also shown is the apparent distribution coefficient.

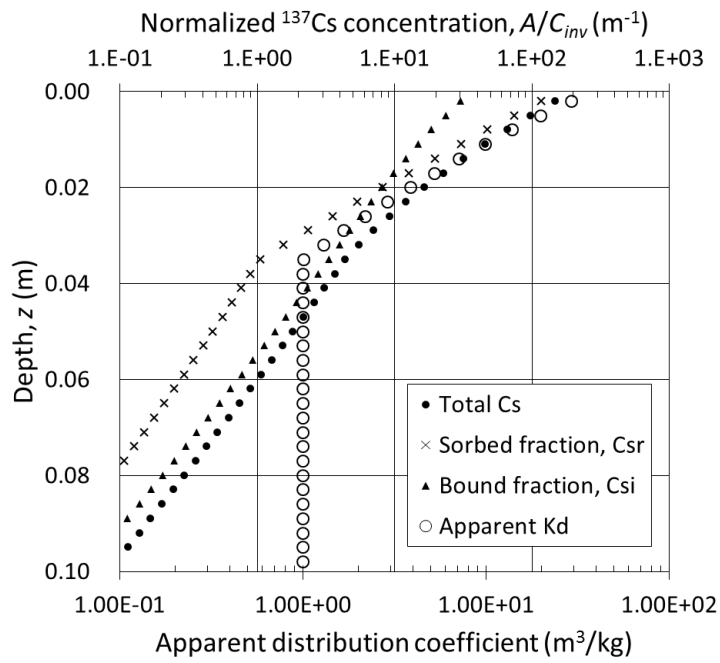
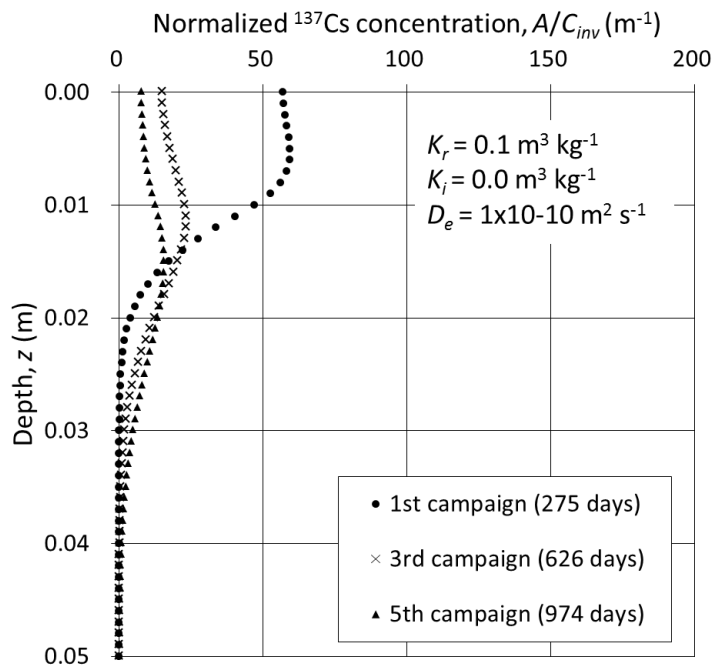


Figure 8 mDSF models capturing the peak in activity below the surface. (a) Low K and low D_e . (b) Low K near the surface (K variable with depth).

(a)



(b)

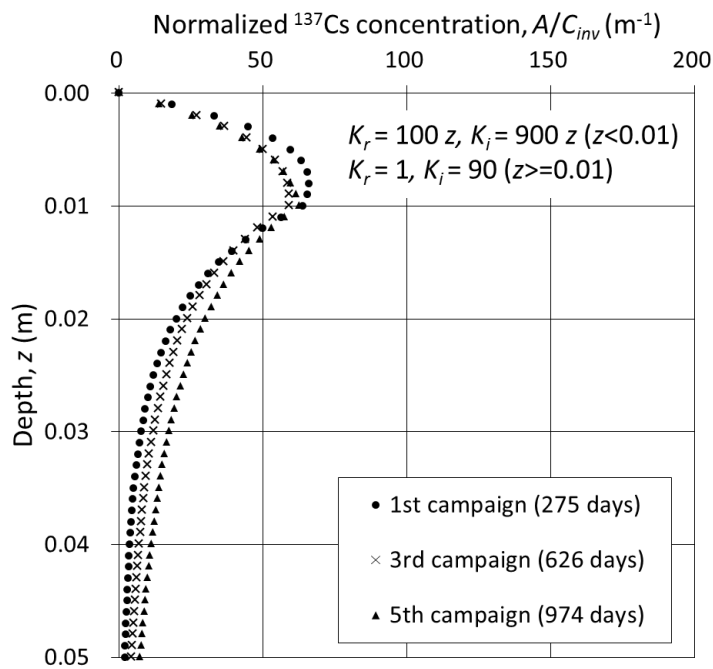


Table 1 One-dimensional physical models for (radio-)contaminants with depth in soil.

Model	Sorption sites	Sorption model (for site 1)	Sorption model (for site 2)	Reversibility	Advection term
Simple Diffusion	1	Instantaneous equilibrium	N/A	Reversible sorption	x
Simple Diffusion with Advection (Bossew and Kirchner, 2004)	1	Instantaneous equilibrium	N/A	Reversible sorption	o
Diffusion-Fixation (DF) (Antonopoulos- Domis et al., 1995)	1	Kinetic model	N/A	One-way fixation	o
Diffusion-Sorption- Fixation (DSF) (Toso and Velasco, 2001)	2	Instantaneous equilibrium	Kinetic model	Reversible for site 1, one-way fixation for site 2	x
Two-Site/Two-Region Models (van Genuchten and Wagenet, 1989)	2	Instantaneous equilibrium	Kinetic model	Reversible for both site 1 and 2	o
Modified Dispersion-Sorption- Fixation (mDSF)	2	Kinetic model	Kinetic model	Reversible for site 1, one-way fixation for site 2	o

Table 2 Parameter values for the reference case.

Symbol	Parameter	Initial value	Reference
K_r	Distribution coefficient for reversible sorption	$1.0 \text{ m}^3 \text{ kg}^{-1}$	Sato (2015), Tsukada et al. (2008)
K_i	Distribution coefficient for irreversible sorption	$9.0 \text{ m}^3 \text{ kg}^{-1}$	
k_{rs}	Sorption rate for reversible site	$1 \times 10^{-6} \text{ s}^{-1}$	Liu et al. (1995), IAEA (2009), Fiengo Perez et al. (2015), Murota et al. (2016)
k_{rd}	Desorption rate for reversible site	$1 \times 10^{-8} \text{ s}^{-1}$	
k_{is}	Fixation rate for irreversible site	$2 \times 10^{-8} \text{ s}^{-1}$	
ε	Porosity	0.5	Characteristic value
S_r	Saturation of pores	0.8	Characteristic value
ρ_d	Dry soil density	950 kg m^{-3}	Characteristic value
v	Darcy velocity	$2 \times 10^{-8} \text{ m s}^{-1}$	Estimated from the annual precipitation intensity in Fukushima
D_e	Effective dispersion coefficient for dissolved cesium	$5.0 \times 10^{-8} \text{ m}^2 \text{ s}^{-1}$	Tuned

Table 3 Different cases in the parameter exploration of the mDSF model. Parameter values which deviate from the initial parameter set are highlighted with asterisks (*) and bold face.

N/A: not applicable.

	Parameter	Unit	Case							
			Reference	High- K	Low- K	No Reverse	No Fixation	Reverse	Low- D_e	No Advection
K_r	Distribution coefficient for reversible fraction	$\text{m}^3 \text{kg}^{-1}$	1.0	*10	*0.1	*0.0	*10.0	*10.0	1.0	1.0
K_i	Distribution coefficient for irreversible fraction	$\text{m}^3 \text{kg}^{-1}$	9.0	*90	*0.9	*10.0	*0.0	*0.0	9.0	9.0
k_{rs}	Sorption rate	s^{-1}	1×10^{-6}	1×10^{-6}	1×10^{-6}	*N/A	1×10^{-6}	1×10^{-6}	1×10^{-6}	1×10^{-6}
k_{rd}	Desorption rate	s^{-1}	1×10^{-8}	1×10^{-8}	1×10^{-8}	*N/A	1×10^{-8}	*1x10⁻⁶	1×10^{-8}	1×10^{-8}
k_{is}	Fixation rate	s^{-1}	2×10^{-8}	2×10^{-8}	2×10^{-8}	2×10^{-8}	*N/A	*N/A	2×10^{-8}	2×10^{-8}
ε	Porosity	-	0.4	0.4	0.4	0.4	0.4	0.4	0.4	0.4
ρ_d	Dry density	kg m^{-3}	1.5×10^3	1.5×10^3	1.5×10^3					
ν	Darcy velocity	m s^{-1}	2×10^{-8}	2×10^{-8}	*0.0					
D_e	Dispersion coefficient	$\text{m}^2 \text{s}^{-1}$	5.0×10^{-8}	*5.0x10⁻⁹	5.0×10^{-8}					